

Efficient Multi-keV X-Ray Sources from Ti-Doped Aerogel Targets

K. B. Fournier,¹ C. Constantin,¹ J. Poco,¹ M. C. Miller,^{1,*} C. A. Back,¹ L. J. Suter,¹ J. Satcher,¹ J. Davis,² and J. Grun³

¹Lawrence Livermore National Laboratory, P.O. Box 808, L-41, Livermore, California 94550, USA

²Alme & Associates, 6020 Richmond Highway, Alexandria, Virginia 22303, USA

³Plasma Physics Division, Naval Research Laboratory, 4555 Overlook Avenue, SW, Washington, D.C. 20375, USA

(Received 21 November 2003; published 23 April 2004)

We have measured the production of $h\nu \approx 4.7$ keV x rays from low-density Ti-doped aerogel ($\rho \approx 3$ mg/cc) targets at the OMEGA laser facility (University of Rochester), with the goal of maximizing x-ray output. Forty OMEGA beams ($\lambda_L = 0.351 \mu\text{m}$) illuminated the two cylindrical faces of the target with a total power that ranged from 7 to 14 TW. The laser fully ionizes the target ($n_e/n_{\text{crit}} \leq 0.1$), and a laser-bleaching wave excites, supersonically, the high-Z emitter ions in the sample. Ti *K*-shell x-ray emission was spectrally resolved with a two-channel crystal spectrometer and also with a set of filtered aluminum x-ray diodes; both instruments provide absolute measurement of the multi-keV x-ray emission. We find between 40 and 260 J of output with $4.67 \leq h\nu \leq 5.0$ keV.

DOI: 10.1103/PhysRevLett.92.165005

PACS numbers: 52.25.Vy, 52.25.Os, 52.50.Jm, 52.70.La

Maximizing the conversion efficiency (CE) of laser energy into multi-keV x rays is a general concern to many areas of high-energy-density plasma physics [1–4]. Bright x-ray sources are needed for backlighters in order to radiograph targets in inertial-confinement fusion (ICF) experiments [3,4]. As the targets get larger, and as compression in the targets increases, the backlighter sources need to be brighter and the backlighter photon energies must increase. To this end, for a given laser power, backlighters can become brighter by becoming more efficient at converting the drive beams to multi-keV x rays. Volumetric heating of low-density gas targets has been shown to be a very efficient method of producing x rays [5]. However, gas targets are limited to a few photon energies (Ar *K*-shell: 3.1 keV, Kr *L*-shell: 1.8 keV, Xe *L*-shell: 4.5 keV, and Kr *K*-shell: 13.3 keV). For a given laser power, the CE also falls off sharply with increasing output x-ray energy [6]. X-ray-yield scaling in solid targets has been studied as a function of laser energy, laser wavelength, laser-pulse length, and focusing properties [7–13]. Historically, solid targets, usually massive disks, have demonstrated efficiencies of only fractions of a percent for multi-keV photon energies. The efficiencies of these massive targets are compromised because much of the laser energy is deposited in a (relatively) low-density region at the critical surface, while the region of the target dominating the radiation output may be a higher-density region that must be conductively heated; steep gradients in solid targets make optimization of the multi-keV source difficult [7]. One hope to increase the efficiency of the solid targets is to heat volumetrically the whole target through a laser-bleaching wave [14].

This Letter presents measurements of x-ray output from laser-heated Ti *K*-shell emitters in a low-density-aerogel plasma. We have achieved a density of $\rho = 3.1 (\pm 0.1)$ mg/cc in our aerogel targets, which gives an ionized density relative to the laser critical density of $0.1n_{\text{crit}}$ ($n_{\text{crit}} = 9 \times 10^{21} \text{ cm}^{-3}$). Previous work with aerogel ma-

terials saw only subsonic heating at a density of $0.6n_{\text{crit}}$ [15]. Other works with low-density (organic) foams have ranged in density from $>0.1n_{\text{crit}}$ to $\sim 0.7n_{\text{crit}}$ [15–18], and they have all seen trans- or subsonic heating and large fractions of the incident energy scattered by parametric instabilities [16,17]. The targets of the present work show supersonic heating, x-ray output 1%–2% of the incident laser energy, and minimal scattering losses.

These experiments were carried out on the OMEGA laser at the Laboratory for Laser Energetics (LLE), University of Rochester. Four targets, at two different densities, were shot at two different laser intensities. The targets for these experiments were doped SiO_2 aerogels with an aggregate density of 3.1 or 3.3 (± 0.1) mg/cc; the SiO_2 aerogel contained 3 at.% Ti. These aerogel targets, when fully ionized, had an electron density that is 8.9 or $9.8 \times 10^{20} \text{ cm}^{-3}$ or ≈ 0.1 times the critical density, n_{crit} , for $0.351 \mu\text{m}$ (3ω) light. The final aerogel material was formed by supercritical extraction of the solvent used to mix the titanium and silicon alkoxides. The density of the aerogel produced is determined by gravimetric analysis of the bulk sample. Analysis by atomic absorption spectroscopy confirmed that the Ti remained at the 3 at.% level after the solvent-extraction process. Visual inspection confirmed that the Ti was uniformly dispersed throughout the sample (no optical scattering centers or crystallites). These doped-aerogel targets are an important step in the development of low-density foams, which are of interest to ICF, shock physics, and radiative transport experiments. The targets were cast in cylindrical Be tubes that had walls $80 \pm 5 \mu\text{m}$ thick. The walls had a transmission $\geq 90\%$ for the Ti *K*-shell x rays ($h\nu > 4.5$ keV) of interest. The cylinders were 2.2 mm long with a 2.0 mm inner diameter, accurate to 3–5 μm . A schematic of our target, laser-beam cones, and the diagnostics used to measure the x-ray output from the target are shown in Fig. 1.

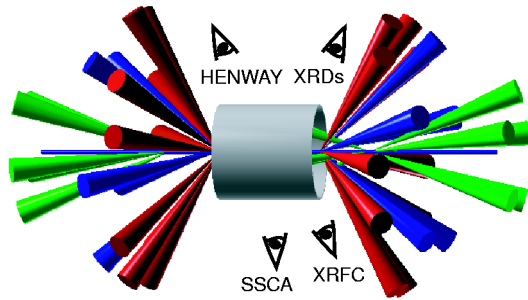


FIG. 1 (color online). Schematic of our target, beam cones, and diagnostics used to measure the Ti x-ray output from the doped foam.

Twenty beams were used in three cones on each face of the target; two shots had both cylindrical faces irradiated, and two shots had irradiation on a single face (see Table I). Beams cones were at 21.4° , 42.0° , and 58.9° to the cylinder axis (henceforth, cones 1, 2, and 3, respectively). The cone 1 beams were focused to $200\ \mu\text{m}$ at a point $1100\ \mu\text{m}$ from the face of the target in order to keep the beam footprints in the Be cylinder; the other two cones are focused to $300\ \mu\text{m}$ at the target face. Differential polarization rotators (DPRs) were employed to smooth all beams. The DPRs increased the stated size of the focal spot for each cone by $70\ \mu\text{m}$. Beams in each cone had a footprint at the target face of ≈ 440 , 475 , and $650\ \mu\text{m}$, respectively. The measured average energies in each beam for each two-sided and each one-sided shot were 180.7 , 362.6 , 380.6 , and $189.0\ \text{J}/\text{beam}$, respectively. One-ns-square pulses were used for irradiating the targets in these experiments. The laser intensities ranged from $I_{\text{Las}} = (1.7\text{--}3.4) \times 10^{15}\ \text{W}/\text{cm}^2$ at the target faces. The dependence of our results on laser intensity and laser energy will be discussed below.

Several diagnostics were used to measure the Ti K -shell output from these targets. The primary measurement was made with a two-channel crystal spectrometer (HENWAY) onto direct exposure film (DEF), both channels employed pentaerthritol crystals. The spectrometer looked at the wall of the target at an angle of 119.1° with respect to the cylinder axis. The known geometry of the spectrometer, crystal reflectivity (measured elsewhere [5]), the attenuation of the differential filters in front of the dispersive crystals, and the known response of the

TABLE I. A summary of the shots in this series of experiments. Columns are OMEGA shot number, target density, laser intensity at the target face, and faces irradiated.

Shot	ρ (mg/cc)	I_{Las} ($10^{15}\ \text{W}/\text{cm}^2$)	Faces irradiated
31047	3.1	1.7	2
31048	3.1	3.3	2
31051	3.3	3.4	1
31052	3.3	1.7	1

DEF [19] are used to compute the energy in a given spectral band. The films were digitized using a microdensitometer with a $22 \times 22\ \mu\text{m}^2$ step size.

The K -shell spectrum for Ti from both channels is shown in Fig. 2. The signal in the H-like Ly_α line at $4.97\ \text{keV}$, as recorded on the higher-energy channel, and the signal in the He-like He_α ($1s2p \rightarrow 1s^2$, $h\nu = 4.75\ \text{keV}$) band ($\Delta E = 0.11\ \text{keV}$ centered at $4.73\ \text{keV}$) found as described below are used to compute the performance of our targets. These spectral windows are similar to what has been reported in the literature for other Ti K -shell x-ray production experiments [8–11].

Photometrically calibrated, filtered aluminum x-ray diodes (XRDs) were also fielded; they returned data on one shot. The diode array viewed the target at the same angle with respect to the cylinder axis as the crystal spectrometer. The diode array has six independent channels filtered to cover the range from 1 to 10 keV. The deconvolved signal from the appropriate channels gives the total power radiated in a given spectral band (see Table II below).

Two-dimensional images of the x-ray emission front in our target were obtained by a gated x-ray framing camera (XRFC). The XRFC was filtered with 16 mil of Be, which gave images of (essentially) pure Ti K -shell emission. The camera images were taken through $50\ \mu\text{m}$ pinholes onto four strips of a microchannel plate; each strip had three images taken approximately 200 ps apart and integrated for 80 ps. The camera had a view at a 63.4° angle with respect to the target axis. A frame from the shot with two-sided illumination ($P_{\text{Las}} = 14.5\ \text{TW}$, $I_{\text{Las}} = 3.3 \times 10^{15}\ \text{W}/\text{cm}^2$) is shown in Fig. 3.

The right edge of the pinholes in Fig. 3 seems to be slightly blocked. The XRFC data are consistent with the rates of axial propagation for the x-ray emission fronts found from filtered x-ray streak camera (SSCA) data [20]

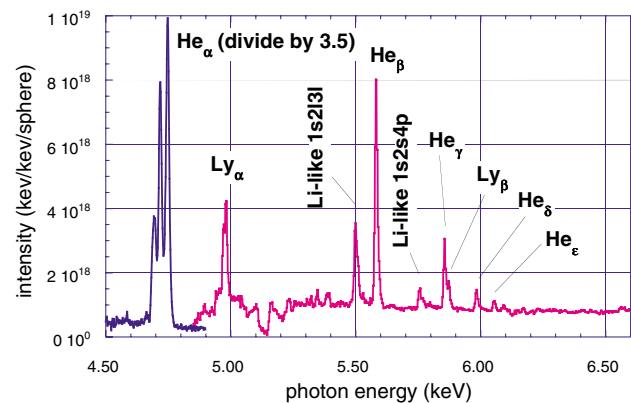


FIG. 2 (color online). Ti K -shell spectrum, in absolute units, from the highest power shot (No. 31048) in our series. The output integrated from 4.67 to $5.0\ \text{keV}$ gives an output equal to 1.9% of the incident laser energy ($14.5\ \text{kJ}$).

TABLE II. Results for x-ray CE measurements: column are shot numbers, measured UV energy delivered to the target, the x-ray CE into $h\nu > 4.7$ keV from DEF, CE into $h\nu > 4.0$ keV from the XRDs, and the prediction from LASNEX.

Shot	E_{UV} (kJ)	CE (%) DEF	CE (%) XRDs	CE (%) LASNEX
31047	7.2	0.8		0.69
31048	14.5	1.9	...	1.26
31051	7.6	1.3	...	0.84
31052	3.8	1.0	1.5	0.48

and showed only minimal curvature of the x-ray front as it moved down the tube.

Since we are interested in maximizing the output of our foam x-ray sources, we measured the energy reflected from the targets with LLE's full-aperture backscatter system. Energy scattered from the target back into the optics of one cone 2 and one cone 3 beam was measured with both a calorimeter and spectrally with a streak camera. The stimulated Brillouin scattering (SBS) signal on the steeper cone 3 beam is a factor of 2–5 larger than on the cone 2 beam, which may be due to an interaction between the steeper cone 3 beam and the Be cylinder wall. The two measurements for the stimulated Raman scattering (SRS) data are within 15%–20% of each other for three of the four shots. The calorimeter-measured energy in the SRS and SBS channels is averaged over the two beam cones. Note, measured energy is only the energy scattered into the $F/6.7$ optic of the two beams used, and our analysis assumes that the scattering on the shallow-angle cone 1 beams is well described by the average of the

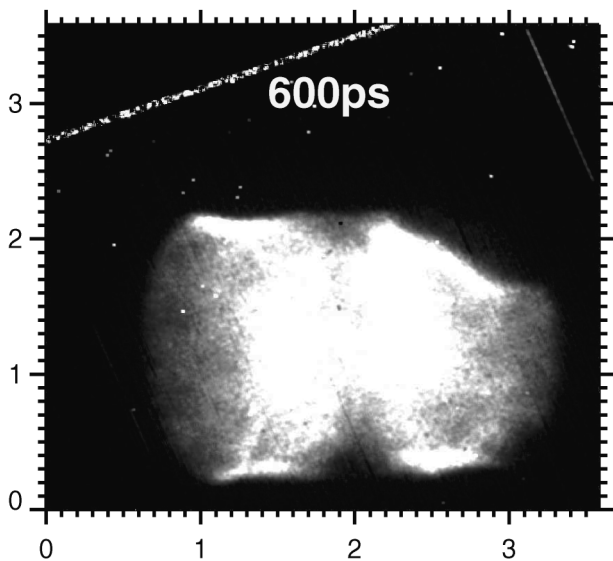


FIG. 3. A frame at 600 ps from the two-sided, high-power shot XRFC data that clearly show the two lobes of plasma before they meet at the center of the cylinder.

measured scattering on the cone 2 and 3 beams. The result is that the target reflects 2.4%–5.2% of the incident energy. The aerogel of the present work is an open-cell foam with cell size estimated to be on the order of 40–50 nm; to the $0.351 \mu\text{m}$ laser pulse, the foam should appear approximately homogeneous [15,16].

We have used LASNEX [21] a 2D, Lagrangian, radiation-hydrodynamics code to simulate these targets. The simulations have three cones of beams onto either one or two faces of the foam cylinder at the appropriate angles. The simulations were run with the average experimental energy per beam and the measured pulse shape for each shot. The resulting peak intensities in the simulations ranged from 1.8×10^{15} – 4.0×10^{15} W/cm^2 . Electron-heat transport in the targets is described by a multigroup flux-limited heat diffusion model based on the Spitzer-Härm thermal conductivity; a flux-limiter value of 0.1 gives the best agreement with the observed heat-front propagation [20]. A finite-element treatment of the electron-heat conduction has been employed; this gives a more accurate solution to the conduction equations for distorted Lagrangian meshes.

From the XRFC images [the high-power two-sided irradiation shot (No. 31048) is shown in Fig. 3] we can see the x-ray emission fronts meeting at the target center by 600 ps after the start of the pulse. This is consistent with the meeting times predicted by LASNEX; the meeting times are later in the lower-power shots. From the gated XRFC images, we demonstrate a fast, volumetric heating of the targets.

The detailed configuration accounting (DCA) atomic physics package was used by LASNEX to compute the radiative emission from silicon, oxygen, and titanium. The DCA atomic physics package [22] solves rate equations for the population in each important excited state in each ionization state. This package is used when accurate atomic physics is needed for line diagnostics. A simple screened hydrogenic model produced the states and transition rates for the present simulations. The optical depths computed for the He_α line in these experiments are $\tau < 0.1$, so the system is optically thin to the Ti x rays.

Table II summarizes the x-ray output measurements for our four shots. The table lists the measured conversion efficiencies relative to the listed energy of each shot (2nd column) found by integrating the DEF (3rd column) from the H-like Ti^{21+} Ly_α transition at ≈ 4.98 keV over a band ± 0.05 keV wide and adding the contribution for the He_α ($1s^2-1s2p^2P$) complex plus its associated satellites. The contribution from the He_α is found by integrating the signal in the He_β ($1s^2-1s3p^2P$) feature and calculating the ratio of He_α to He_β with a detailed collisional-radiative model (CRM) [23,24]. The ratio of energy in He_β to He_α varies by 10% between 2 and 3 keV, the range of plasma temperatures predicted by LASNEX. The whole series of He-like and H-like lines visible in Fig. 2 are fit with a single-temperature spectrum; the ratio of He_α to

He_β from the model at that best-fit temperature is then used to compute the contribution of He_α to the total Ti K -shell signal. Shots 31047 and 31051 were fit very well for $T_e = 2.25$ keV ($\text{He}_\alpha/\text{He}_\beta = 8.94$), while shots 31048 and 31052 were fit at $T_e = 3.0$ and 2.0 keV ($\text{He}_\alpha/\text{He}_\beta = 8.53$ and 9.47), respectively. The relative strength of He_α to He_β is then checked for consistency with the Ti spectrum measured in the lower-energy channel of the spectrometer. The ratios of He_α to He_β observed in the lower-energy channel are within $\approx 40\%$ of these numbers. As stated above, the measured scattering energy losses from the targets are $\lesssim 5\%$. The CE numbers in Table II reflect this small correction to the incident laser energy.

There is an overall $\pm 30\%$ uncertainty on the CE numbers measured with the DEF that results from measured uncertainties in crystal reflectivity across the width of the crystal [5], relative transmissivity of differential filters, and the level of film background. The signal measured with the XRDs in the band from 4 to 6 keV for shot 31052 is also listed; there is a $\pm 20\%$ error bar on the deconvolved XRD signal. The XRD signal contains the contribution from the higher- n members of the He- and H-like Rydberg series. Aside from He_β , their contributions are negligible. The contribution from He_β , based on our CRM, is $\approx 10\%$. The measured CE for shots 31047 and 31051, given the $\pm 30\%$ uncertainty quoted, were $\approx 1/2$ that of No. 31048; this scales directly with the total energy delivered to the target. However, there is not a drop in CE for No. 31052, which had $\approx 50\%$ of the energy of 31047 and 31051. The laser intensity on each face of the target was a factor of 2 greater in No. 31051 than No. 31047 (3.4×10^{15} versus 1.7×10^{15} W/cm²). The resulting CEs seem only slightly dependent on intensity in this case.

Also listed in Table II is the prediction for the x rays out from our targets from LASNEX; the Ti spectrum in the simulation is integrated from 4.4 keV up to 5.1 keV, thus including the He_α and Ly_α lines. The CE numbers from the DCA runs are listed in the last column of Table II. In every case, the targets appear to perform better than predicted by the simulations.

In summary, this Letter reports on the output of $\approx 1.0\% - 2.0\%$ of the incident laser energy in the 4.67–5.0 keV band, measured with a x-ray crystal spectrometer, from a low-density Ti-doped aerogel target. Output of 1.5% is measured in the 4–6 keV band with filtered x-ray diodes. The targets contained 3 at. % Ti in SiO_2 aerogel, which when fully ionized had electron densities in the range $0.1n_{\text{crit}}$. Supersonic, volumetric heating of the targets results in efficient conversion of the laser energy into x rays. The supersonic heating by the laser-drive beams is complimented in our low-density targets by low levels ($\lesssim 5\%$) of laser-scattering energy losses.

Finally, we note that previous work has found CEs for Ti targets that ranged from 0.01%–0.6% [8–11] for lasers at 2ω and 3ω (0.53 and 0.35 μm) with pulse lengths 100–500 ps. The targets of the present work were irradiated with ns-scale pulses: these targets performed between 50% and a factor of 3 better than the results reported by Yaakobi *et al.* [8], which are the highest published CEs for Ti that we have found. The improvement in performance for our targets compared to those of Yaakobi *et al.* scales nearly linearly with the increase of laser intensity above that of Yaakobi *et al.* Much work remains to be done developing and optimizing the low-density, doped-foam targets as bright, efficient x-ray sources.

This work was performed under the auspices of the U.S. Department of Energy by the University of California Lawrence Livermore National Laboratory under Contract No. W-7405-Eng-48.

*Permanent address: Los Alamos National Laboratory, P.O. Box 1663 MS E540, Los Alamos, NM 87545, USA.

- [1] N. C. Woolsey, D. Riley, and E. Nardi, *Rev. Sci. Instrum.* **69**, 418 (1998).
- [2] F. Ze *et al.*, *J. Appl. Phys.* **66**, 1935 (1989).
- [3] S. G. Glendinning *et al.*, *Phys. Plasmas* **7**, 2033 (2000).
- [4] S. R. Goldman *et al.*, *Phys. Plasmas* **6**, 3327 (1999).
- [5] C. A. Back *et al.*, *Phys. Rev. Lett.* **87**, 275003 (2001).
- [6] R. Kauffman, in *Handbook of Plasma Physics*, edited by A. M. Rubenchik and S. Witkowski (Elsevier, Amsterdam, 1991), Vol. 3, p. 111.
- [7] R. Kodama *et al.*, *J. Appl. Phys.* **59**, 3050 (1986).
- [8] B. Yaakobi *et al.*, *Opt. Commun.* **38**, 196 (1981).
- [9] D. L. Matthews *et al.*, *J. Appl. Phys.* **54**, 4260 (1983).
- [10] D. W. Phillion and C. J. Hailey, *Phys. Rev. A* **34**, 4886 (1986).
- [11] G. J. Tallents *et al.*, *J. Quant. Spectrosc. Radiat. Transfer* **43**, 53 (1990).
- [12] G. A. Kyrala *et al.*, *Appl. Phys. Lett.* **60**, 2195 (1992).
- [13] J. Workman and G. A. Kyrala, *Rev. Sci. Instrum.* **72**, 678 (2001).
- [14] J. Denavit and D. W. Phillion, *Phys. Plasmas* **1**, 1971 (1994).
- [15] J. A. Koch *et al.*, *Phys. Plasmas* **2**, 3820 (1995).
- [16] K. A. Tanaka *et al.*, *Phys. Fluids* **28**, 2910 (1985).
- [17] H. Figueroa, C. Joshi, and C. E. Clayton, *Phys. Fluids* **30**, 586 (1987).
- [18] V. V. Gavrilov *et al.*, *Quantum Electron.* **31**, 1071 (2001).
- [19] B. L. Henke *et al.*, *J. Opt. Soc. Am. B* **3**, 1540 (1986).
- [20] C. Constantin *et al.*, *Phys. Rev. Lett.* (to be published).
- [21] G. Zimmermann and W. Kruer, *Comments Plasma Phys. Controlled Fusion* **2**, 51 (1975).
- [22] Y. T. Lee, *J. Quant. Spectrosc. Radiat. Transfer* **38**, 131 (1987).
- [23] S. H. Glenzer *et al.*, *Phys. Rev. E* **62**, 2728 (2000).
- [24] C. Biedermann, R. Radtke, and K. B. Fournier, *Phys. Rev. E* **66**, 066404 (2002).